Electron Cyclotron current drive studies on KSTAR using imaging MSE

C.A. Michael[1], A. Thorman[1], J. Chung[2], YS Bae[2],

J. H. Jeong[2], J. Decker[3], J. Howard[1]

[1] *Australian National University, Canberra, A.C.T.,2601, Australia*

[2] *National Fusion Research Institute, Daejeon, Republic of Korea*

[3] *CRPP, Lausanne, Switzerland*

The production of non-inductive current drive through electron cyclotron resonance is one candidate method for long pulse plasma sustainment. Electron cyclotron current drive systems have been deployed on tokamaks worldwide, including DIII-D, ASDEX and TCV. Several codes for modelling the current drive efficiency have been developed, and are continuously being improved. There are to date, however, only a few cases where these codes have been benchmarked against measurements. The net current produced by electron cyclotron current drive (ECCD) can be inferred from external magnetics, as well as temperature measurements (to model the resistivity). This technique was used in DIII-D [1], and also in in demonstrating full non-inductive scenarios produced by ECCD in TCV [2].

As demonstrated on both DIII-D [3], motional Stark effect (MSE) measurements provide a far superior method for distinguishing the non-inductive ECCD currents. In this paper, the ECCD induced changes in core current are measured using an imaging MSE System (IMSE) [4-6] installed on the KSTAR tokamak. Imaging MSE allows a 2D map of the vertical magnetic field distribution to be obtained, up to the extent of the height of the neutral beam. Experiments were undertaken at total constant current using the 170GHz (700kW) gyrotron [7], modulated at 2-2.5Hz, in various combinations and launch directions (co and counter), and at various field strengths including deposition near the magnetic axis in plasmas with sawtooth instabilities.

Electron cyclotron resonance heating and current drive ECH/CD is also known to have an effect on sawteeth, which redistribute heat and current to regions outside the sawtooth inversion radius. ECH/CD-induced changes in sawteething may also cause a net average reduction in the current inside the sawtooth inversion radius, and reduce the non-inductive ECCD current.

The evolution of current and loop-voltage is governed by the current diffusion equation. The heating promptly decreases the resistivity η and reduces the loop voltage and flux consumption, in addition to the effects of the driven non-inductive current, which appears only after the resistive timescale $\tau=\mu_0/\eta l^2$, where l is the length scale of the current perturbation. For a typical value of l=5cm with T_e =1.5keV, Z_{eff}=2, we get τ=150ms. As the total current is held constant in these experiments, any current driven in the core will be compensated by a "back-reaction current" elsewhere in the plasma.

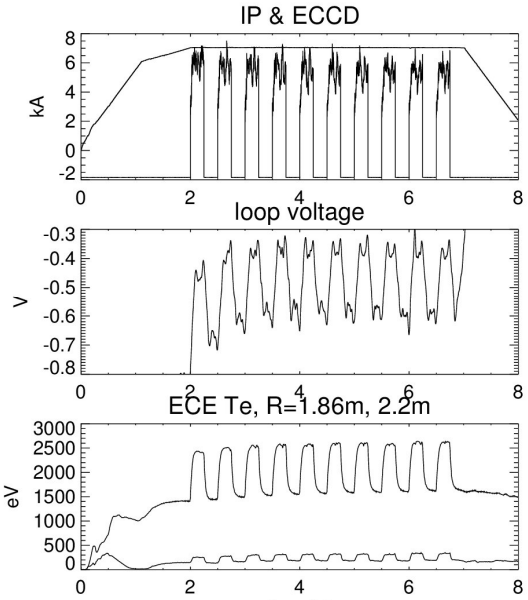

Figure 1: Waveforms of current, ECCD power, loop voltage, core and edge electron temperature for co-injected shot #9323

ECCD Modulation experiments

To detect the small change in pitch angle due to ECCD, the power was modulated at 2-2.5Hz (slower than the current diffusion time) for 6-8 cycles. Waveforms of the current, ECCD power, and loop voltage and edge/core T_e are plotted in Fig. 1, for a shot with co ECCD at 3.0T, which has a resonance position on axis (R=1.8m). It is clear that the loop voltage drops upon ECCD, however, as the edge temperature increases, the loop voltage change may be attributable to a change in resistivity alone. Thus it is difficult to conclude about the direction or magnitude of the driven current. An image of the time/space history of the MSE polarization, angle on the midplane, for the same shot, is shown in Fig 2. The ECCD waveform modulation has a clear signature in the MSE data.

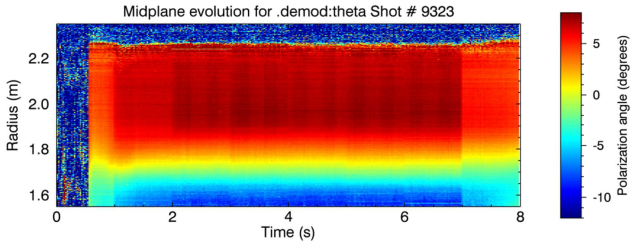

Figure 2: Evolution of IMSE mid-plane pitch angle as a function of time for discharge shown

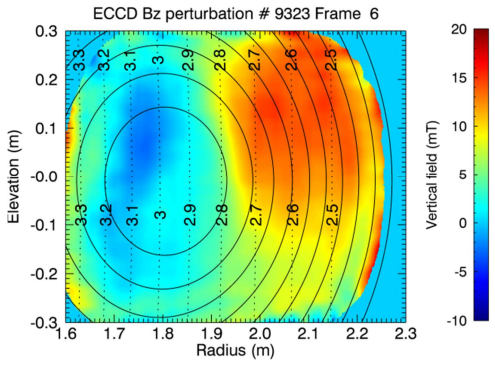

Figure 3: Cycle-averaged perturbation in Bz from IMSE, 150ms after ECCD switch on.

A 2D image of the change in B_z, inferred from MSE, averaged over 6 modulation cycles, compared with the magnetics-constrained EFIT flux surfaces and |B| contours, is shown in Fig. 3. The vertical field exhibits large changes around R=1.9m and 1.6m. A component of the current density can be obtained from the radial derivative in B_z, and is shown in Fig. 4, as a function of time and space. The current density is seen to respond over a timescale of ~100ms, and has a major peak around R=1.9m, which is 10cm away from the cold resonance. This may be due to the resonance of the "hot electrons" giving rise to a Doppler shift. Furthermore, there is a "negative" current peak around R=1.6m. This unexpected peak indicates that there may be a shift in the equilibrium. Such a shift would not be unexpected, due to a change in the Shafranov shift, as the stored energy increases ~30% upon ECCD application. In the above-mentioned discharge, the Shafranov shift is being opposed by the vertical field control system to attempt to maintain constant plasma position, however, there would still be a relative displacement of different surfaces, due to a change in the pressure profile. Thus, while the (R,Z) coordinate system is appropriate for comparison with the resonance condition, a flux coordinate system (ρ) is more appropriate under this strong pressure change.

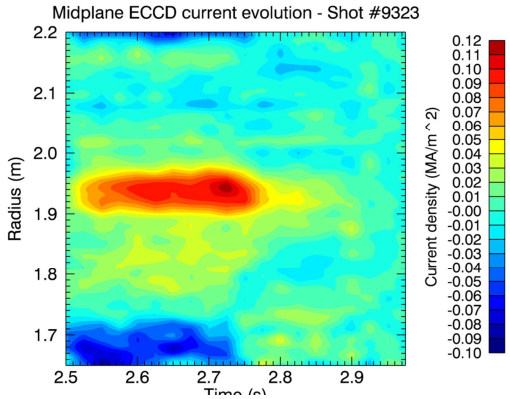

Figure 4:Spatio-temporal evolution of current density on midplane, formed from cycle average of 6 ECCD pulses.

Enclosed current perturbation in co and counter-ECCD discharges

Using the integral form of Ampere's law, and using a fixed EFIT reconstruction for estimation of the mapping ρ(R), a perturbation analysis reveals that the change in enclosed current as a function of flux label can be well approximated from the in-out asymmetry of the field perturbation: $\delta I(\rho) = 2\pi r(\rho)(\delta B_{out}(\rho) - \delta B_{in}(\rho))$. However, this is only possible for inner radii down to the beam tangency radius and IMSE field of view (effectively limiting this analysis to ρ=0.3-0.4 as seen in Fig. 3). The profile of the amplitude and phase of the fundamental component of the perturbed current is plotted in Fig. 4. The net current is in the co direction, and lags in phase by approx. 90 degrees in the region ρ>0.2. This long delay is characteristic of the resistive timescale, suggesting this is truly non-inductive current. Also, the current may yet not have reached equilibrium. The magnitude of the enclosed current is

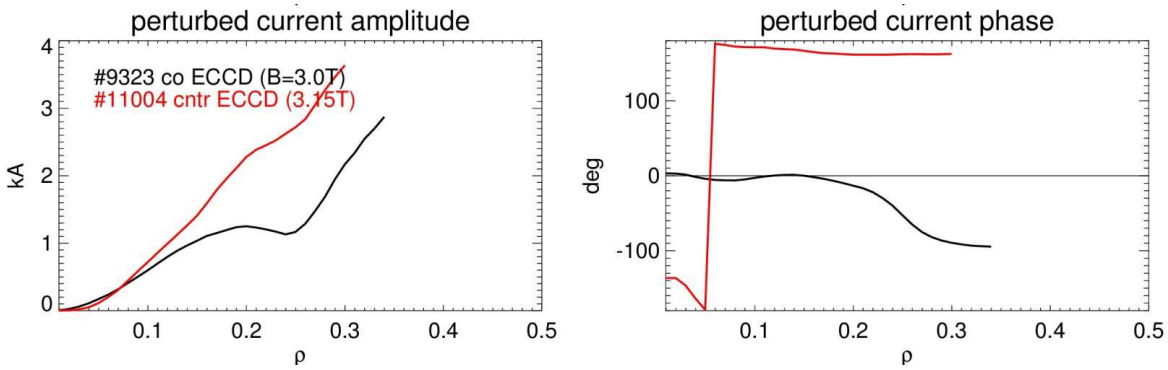

Figure 4: Amplitude and phase of fundamental component of the fundamental enclosed current perturbation in discharges with co (black) and counter (red) injection

reaches a maximum of ~3kA at ρ=0.3, possibly increasing at larger radii. Theoretical estimates based on the pre-computed current drive efficiency tabulated at ρ=0 [7] give values around 8kA total driven current. Whilst sawteeth instabilities may broaden the induced current profile, sawteeth were stabilized by ECCD in this discharge. Also in Fig. 4 is plotted the derived perturbed current profile for a shot with counter ECCD injection at 2Hz. There is a 180-160 deg phase lead, indicating a counter current, as expected.

An additional case with co-injection into an H-mode discharge at 2.0T has a magnitude of ~10kA at ρ=0.3, with phase lag of ~160 deg everywhere, indicating a dominantly counter injection behaviour. This unexpected behaviour might be caused by a change in the sawtooth behaviour during the application of ECCD in this case.

The complete response of the plasma will be modelled with the ray tracing and Fokker-Planck codes CPO/LUKE, including the effects of sawtooth and current diffusion. Future experiments will focus on changing the sawtoothing characteristics, and deposition location with respect to the sawtooth inversion radius, to better understand this effect.

1. James, R.A., G. Giruzzi, B. Degentile, L. Rodriguez, et al., Physical Review A, 1992. **45**(12): p. 8783-8786.
2. Sauter, O., C. Angioni, S. Coda, P. Gomez, et al., Physics of Plasmas (1994-present), 2001. **8**(5): p. 2199-2207.
3. Petty, C.C., R. Prater, J. Lohr, T.C. Luce, W.R. Fox, R.W. Harvey, J.E. Kinsey, L.L. Lao, and M.A. Makowski, Nuclear Fusion, 2002. **42**(12): p. 1366-1375.
4. Howard, J., Plasma Physics and Controlled Fusion, 2008. **50**(12): p. 125003.
5. Chung, J., J. Ko, J. Howard, C. Michael, G.v. Nessi, A. Thorman, and M.D. Bock, Journal of the Korean Physical Society, 2014. **65**(8): p. 1257-1260.
6. Thorman, A., C. Michael, and J. Howard, Review of Scientific Instruments 2013. **84**: p. 063507.
7. Bae, Y.S., M. Joung, H.L. Yang, W. Namkung, M.H. Cho, H. Park, R. Prater, R.A. Ellis, and J. Hosea, Fusion Science and Technology, 2011. **59**(4): p. 640-646.